



RESEARCH ARTICLE

VIRTUAL DESIGN OF NOVEL OF ORALLY BIOAVAILABLE PIPERAZINE INHIBITORS OF ENOYL-ACYL CARRIER PROTEIN REDUCTASE OF MYCOBACTERIUM TUBERCULOSIS WITH FAVORABLE PHARMACOKINETIC PROFILES

Koffi Charles Kouman¹, Affiba Florance Kouassi¹, Yves Kily Hervé Fagnidi^{1,2}, Issouf Fofana¹, Koffi N'Guessan Placide Gabin Allangba^{1,3,4,5}, Méralie Kéita¹, Eugene Megnassan^{1,6,7,8,9}

¹Applied Fundamental Physics Laboratory (LPFA), Nangui Abrogoua University, Ivory Coast. ²Science and Technology Training and Research Unit, Alassane Ouattara University, Ivory Coast. ³Laboratory of Environmental Sciences and technologies, Jean Lorougnon Guédé University, Ivory Coast. ⁴Laboratory of Biophysics and Nuclear Medicine (LBNM), Félix Houphouët-Boigny University, Ivory Coast. ⁵Department of Medical Physics, University of Trieste and International Centre for Theoretical Physics (ICTP), Trieste, Italy. ⁶Laboratory of Structural and Theoretical Organic Chemistry, Félix Houphouët-Boigny University, Ivory Coast. ⁷International Center for Theoretical Physics, ICTP-UNESCO, Coastal Road 11, I-34151 Trieste, Italy. ⁸International center for applied research and sustainable technology, SK-84104 Bratislava. ⁹Laboratory of Crystallography-Molecular Physics, Félix Houphouët-Boigny University, Ivory Coast.

Article Info:



Article History:

Received: 21 July 2024
 Reviewed: 13 September 2024
 Accepted: 20 October 2024
 Published: 15 November 2024

Cite this article:

Kouman KC, Kouassi AF, Fagnidi YKH, Fofana I, Allangba KNPG, Kéita M, Megnassan E. Virtual design of novel of orally bioavailable piperazine inhibitors of enoyl-acyl carrier protein reductase of *Mycobacterium tuberculosis* with favorable pharmacokinetic profiles. Universal Journal of Pharmaceutical Research 2024; 9(5): 91-104.

<http://doi.org/10.22270/ujpr.v9i5.1216>

*Address for Correspondence:

Yves Kily Hervé Fagnidi, Applied Fundamental Physics Laboratory (LPFA), Nangui Abrogoua University, Ivory Coast. Science and Technology Training and Research Unit, Alassane Ouattara University, Ivory Coast. Tel: +225-01-02-90-66-85; E-mail: kfagnidi@yahoo.fr

Abstract

Background: Drug-resistant strains have been a real problem for anti-tuberculosis therapies in recent decades. Here we elaborated the virtual rational design and evaluation of a novel class of piperazine (PPZ) analogs as InhA-Mt inhibitors with a favorable pharmacokinetic profile.

Method: By *in situ* modification of the crystal structure of InhA-PPZ1 (Protein Data Bank (PDB) entry code: 1P44), which is the reference structure of a test set of 12 PPZs with their known inhibitory potencies experimental data (IC₅₀^{EXP}), we prepared three-dimensional (3D) models of InhA-PPZx complexes. A structure activity relationship (SQR) model was built in the gas phase in the search for active conformations of PPZ 1-12 linearly correlating the calculated enthalpy of formation of the InhA-PPZ complex and the IC₅₀^{EXP}. Finally Lipinski's rule of 5 was used to filter the VCL which was subsequently screened by the pharmacophore model. The predicted activities of the new PPZ analogs obtained were evaluated with the initial QSAR and their pharmacokinetic profile was also evaluated.

Results: The virtual combinatorial library of more than 310,550 PPZ analogs was filtered by Lipinski's rule until it reached 19,044 analogs. Virtual screening by the pharmacophore made it possible to select 50 potential new analogues with predicted inhibitory potencies up to 100 times better than that of PPZ1 (IC₅₀^{EXP}=160 nM). The predicted pharmacokinetic properties of the new analogues showed high cell membrane permeability, side effects and high human oral absorption compared to current anti-TB candidates.

Conclusions: The combined use of molecular modeling and PH4 in virtual screening makes it possible to propose new powerful anti-tuberculosis drugs with favorable pharmacokinetic profiles.

Keywords: ADME, InhA inhibitors, Piperazine, pharmacophore, QSAR, tuberculosis, virtual screening.

INTRODUCTION

Tuberculosis is as old as humanity itself. It has afflicted kings and queens, poets and politicians, revolutionaries and writers, activists and actors. Most of its victims, however, are poor, marginalised or malnourished, and the out-of-pocket costs associated

with treating TB expose them to financial hardship or drive them further into poverty. TB is the definitive disease of deprivation. Turning the tide on TB means screening and treatment for those it strikes, and preventing it by addressing its drivers and developing a new vaccine. Only by working together can we turn the tide against this ancient killer is the position of the Dr.

Tedros Adhanom Ghebreyesus, Director-General of World Health Organization according the 2024 WHO report¹. We can prevent and curate tuberculosis disease. But in 2023 tuberculosis disease will probably once again become the main cause of death due to a single infectious agent in the world, after 3 years during which it was the corona virus (COVID 19) which was the primary cause and which caused approximately twice as many deaths compared to HIV/AIDS. Every year, more than 10 million people continue to contract tuberculosis and this has been increasing since 2021¹. The World Health Organization (WHO) and United Nations (UN) Member States have adopted urgent action to end the global tuberculosis epidemic by 2030¹. Recent decades have seen no new anti-tuberculosis drugs on the market despite the increasing incidence of tuberculosis worldwide and the threat to public health. Bedaquiline, a new antimycobacterial, approved at the end of 2012² inhibits adenosine 5'-triphosphate (ATP)-synthase of *Mt*b with good clinical efficacy against multiple resistant strains. However, this drug has cardiovascular side effects³.

Diversification of mycobacterial drug targets is therefore imperative in combating the increasing incidence of drug-resistant *Mt*b strains. The synthesis of type II fatty acids (FAS-II system) of *Mt*b is ensured by the key role of the oxidoreductase activity of the carrier protein enoyl-acyl reductase (InhA or ENR). The elongation cycle of mycolic biosynthesis is catalyzed by this essential enzyme which is an essential element of the mycobacterial cell wall⁴. InhA is a promising drug target and is validated by anti-tuberculosis agents. Additionally, the WHO Special Program for Research and Training in Tropical Diseases (TDR) has listed it in its target database as an attractive pharmacological target for the design of new drug candidates^{5,6}. "The term totally resistant (TDR-TB) has emerged to mean infection with a strain resistant to all first- and second-line drugs"⁷. As a prodrug, the isoniazid (INH) molecule is used as a first-line drug in the prevention and treatment of tuberculosis. INH, activated by the bacterial catalase-peroxidase enzyme (KatG), couples isonicotinic acyl with the reduced form of nicotinamide adenine dinucleotide (NADH) forming an isonicotinic acyl-NADH complex. This complex binds tightly to InhA, blocks the natural substrate and prevents the action of fatty acid synthesis, which hinders mycolic acid synthesis⁸. In the fight against multidrug-resistant (MDR-TB), extensively drug-resistant (XDR-TB) and total drug-resistant (TDR) tuberculosis. -TB", major interest is therefore focused on compounds which can directly inhibit InhA without requiring activation by KatG⁹. The discovery of inhA inhibitors that do not require KatG activation is a research activity of several working groups based on different scaffolds: triclosan⁹, diphenyl ether^{10,11}, pyrrolidinecarboxamide¹², arylamide derivatives¹³, benzamide derivatives with Tyr158 'out' conformation and interaction with the Phe41 and Arg43 pocket instead of the stacking with Phe97¹⁴, thiadiazole-based InhA inhibitors and Piperazine derivatives with Tyr158 'out' conformation and interaction with NADH cofactor¹⁵. Each of its

different compounds displays intermediate inhibitory power. Studies show that a potent InhA inhibitor should be a relatively long molecule that binds InhA adjacent to the NADH cofactor binding site. Also this inhibitor should have a bulky group that selectively inserts into a hydrophobic pocket of InhA constituted by residues Met155, Pro193, Ile215, Leu217, Leu218 and Trp222 located near a larger cavity accessible to the solvent¹⁶. The main objective of this work was the design of novel potent nanomolar inhibitors of 1-(9H-fluoren-9-yl)-piperazine (PPZ) based on a series of 12 compounds (training set) and 3 other compounds (validation set) nanomolar inhibitors with inhibitory potencies observed as low as $IC_{50}^{exp}=160\text{ nM}$ ¹⁶. From the *in situ* modification of the crystal structure of the InhA-PPZ1 complex (PDB: 1P44), we have developed a QSAR model which correlates the Gibbs free energies of the formation of the InhA-PPZx complexes with the IC_{50}^{exp} powers and we have determined the active conformations of PPZs bound to the active site of Mt InhA (MM-PB complexation approach). Based on the active conformations of the inhibitors in the test set, we established a 3D QSAR activity pharmacophore of InhA (PH4) inhibition. Subsequently we generated a large virtual library of compounds sharing the PPZ scaffold and this was screened *in silico* with PH4. The virtual screening led to inhibitor results that exhibited predicted inhibitory potencies IC_{50}^{pre} more than 100 times lower than that of the most active test set compound PPZ1. Finally, the selected hits were subjected to complexation simulations to evaluate the inhibitory activity predicted for the best analogues and to calculate their ADMET profile.

MATERIAL AND METHODS

Structural studies and bioassays (IC_{50}^{exp}) of our studied piperazines derivatives (PPZ) InhA inhibitors were taken from literature¹⁶. The efficacy range of inhibitory concentrations ($160 \leq IC_{50}^{exp} \leq 51000\text{ nM}$), allows us to realize QSAR models. The whole series of 15PPZs were divided into a training (TS) and a validation (VS) sets of 12 and 3PPZs respectively¹⁶.

Model building

The whole complex (E:I), with free InhA (E) and inhibitor (I) was resolved to a reliability factor of 1.7 Å containing the Genz-10850 (PPZ1) bound to InhA (Whose crystallographic data entry code 1P44^{17,18} from Discovery Studio 2.5 software¹⁹. Virtual design plan to result in new PPZ analogs with higher predicted activity is presented in scheme 1. The structures (E and E:I complexes) were at the neutral pH=7 and neutral N- and C-terminal residues, all protonizable and ionizable aminoacids being charged, without any crystallographic water molecules. The inhibitors were built into the 1P44 structure by *in situ* replacing derivative groups of the PPZ1 moiety followed by systematic conformational search of the replacing group coupled with a careful energy minimization of the modified inhibitor and surrounding InhA active site residues²⁰⁻³⁵.

Molecular mechanics

Molecular mechanics using the CFF97 force field allowed the modeling of inhibitor complexes, InhA and E-I²⁸ as described previously²⁸.

Conformational Search

For conformational research we recommend reading the following articles^{21,30,36}.

Solvation Gibbs free energies

As for the free solvation energy has been described perfectly by the following articles³⁰.

Calculation of Binding Affinity and QSAR Model

The GFE calculation of the binding affinity expressed as complexation has been detailed earlier²⁸.

Interaction energy

For interaction energy refer to the full description we reported formerly^{13,24,25}.

Pharmacophore generation

From the E-I complex models, we used the bound conformations of the inhibitors to construct a 3D-QSAR pharmacophore model (PH4) using the Catalyst HypoGen algorithm¹⁹ implemented in Discovery Studio¹⁹ as described earlier²⁸.

Virtual library generation

The virtual library was generated according to the method described previously²⁸.

ADME properties

The drug similarity selection criterion was used to target the initial virtual library, as previously described²⁸.

Pharmacophore-based library searching

Derived from the bound conformations of PPZs at the active site of InhA, the pharmacophore model (PH4) as presented in the "Pharmacophore generation" section served as a library search tool as previously described²⁸.

Inhibitory potency prediction

The conformer with the best mapping on the PH4 pharmacophore in each cluster of the focused library subset was used for $\Delta\Delta G_{com}$ calculation and IC₅₀ pre estimation (virtual screening) by the complexation QSAR model as described earlier³⁷.

RESULTS

Training and validation sets

A heterogeneous series of InhA inhibitors was selected with their known and experimentally determined inhibitory activities coming from the same laboratory (Table 1), constitutes the training set consisting of 12 PPZs and the validation set consisting of 3 other analogues¹⁶. First, 1-(9H-fluoren-9-yl)-piperazine was synthesized bearing modifications around the carbonyl hydrogen bond acceptor. Using 1-(9H-fluoren-9-yl)-piperazine (3), compounds 2 and 4 to 8 were synthesized in low yields. Additionally, direct sulfonylation was used for the synthesis of benzenesulfonyl derivatives 5a – b to obtain the desired products¹⁶. The entire series was obtained by five-position variations of the substituents on the phenyl rings in Table 1. Experimental concentrations at half maximum inhibition ($160 \leq IC_{50}^{exp} \leq 51,000$ nM)¹⁶ cover a wide range of concentrations sufficiently extend for building a reliable QSAR model.

One descriptor QSAR models

From the model of the refined crystal structure (pdb entry code: 1P44)¹⁶ we prepared by *in situ* modification each InhA-PPZx complex (Table 1) of the training set (TS) numbering 12 and those of the validation set (VS) numbering of 03 as described in the Method section. We thus calculated for each of the 15 optimized enzyme-inhibitor complexes the relative Gibbs free energy of the formation of the InhA-PPZx complex ($\Delta\Delta G_{com}$). The calculated values $\Delta\Delta G_{com}$ and its components as described previously²⁸ are presented in table 2 for the TS and VS of piperazine¹⁶. The QSAR model explained variation in the PPZs experimental inhibitory potencies ($pIC_{50}^{exp} = -\log_{10}(IC_{50}^{exp})$)¹⁶ by correlating it with computed GFE $\Delta\Delta G_{com}$ through linear regression (eq. B), Table 2. The complexation enthalpy $\Delta\Delta H_{MM}$ was calculated in the gas phase and then correlated with pIC_{50}^{exp} to seek better insight into the binding affinity of PPZs toward MtInhA. The effect of the solvent and the loss of entropy of the inhibitor during its binding to the enzyme not being initially taken into account, the validity of this linear correlation (for statistical data from the regression (Table 3) made it possible to evaluate the importance of inhibitor-enzyme interactions ($\Delta\Delta H_{MM}$). This correlation explains approximately 88% of the variation in the pIC_{50}^{exp} data and shows the significant role of the enthalpy contribution in the binding affinity of the ligand to the active site. Likewise, the more advanced descriptor, namely the GFE of the InhA-PPZx complex formation containing all components: $\Delta\Delta H_{MM}$, $\Delta\Delta TS_{vib}$ and $\Delta\Delta G_{sol}$, has been evaluated (Table 3). The large relationship between the 3D model of inhibitor binding and the observed inhibitory potencies of PPZs is explained by the relatively high values of the regression coefficient R², the cross-validated regression coefficient R²_{xv} and the Fischer F test of the correlation suggests¹⁶. Therefore, the active conformation of PPZs bound to the InhA binding site allowed the generation of the PH4 pharmacophore and access to structural information derived from the 3D models of InhA-PPZx. These complexes can then be expected to lead to a reliable prediction of InhA inhibitory potencies for new PPZ analogues, based on the QSAR B model, Table 3. The validity of the correlation equations (A) and (B) illustrated in Figure 1 are confirmed by the statistical data. The $pIC_{50}^{pre}/pIC_{50}^{exp}$ ratio $\cong 1$ (pIC_{50}^{pre} values were estimated using correlation equation B, Table 3) calculated for the entire PPV13-15 validation set documents the substantial predictive power of the QSAR model complexation of table 2. Thus, the regression equation B (table 3) and the calculated GFE $\Delta\Delta G_{com}$ can be used to predict pIC_{50}^{pre} inhibitory potencies against MtInhA for novel PPZ analogs, provided they share the same binding mode as the entire PPZ1-12 piperazine test set.

Binding mode of PPZs

In the crystal structure of InhA –PPZ1¹⁶ the substitution at R-groups of the piperazine derivative scaffold of the inhibitor sits in a hydrophobic cavity of the active-site surrounded by side chains of

predominantly non polar residues: Pro 99, Gly 104, Met103, Tyr158, Phe149 and Met161, Met 98, Ala 198. According to the structures of PPZ8 and PPZ5 studied by docking simulations, the presence of the methyl group at the C2 position of the aryl moiety causes steric hindrance due to the restricted space in the cavity formed by Met103, Tyr158, and Met161 residues of MtInhA. In contrast to the recently reported methyl thiazoles that interact with MtInhA in a “Tyr158-out” binding mode direct inhibitors such as pyrrolidinecarboxamides³⁸ and piperazine-indole derivatives³⁹ have explored polar interactions involving a ribose hydroxyl, the Tyr158 hydroxyl and a hydrogen bond acceptor in the compounds.

Interaction Energy

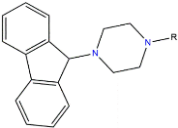
Additional key structural information was given by the interaction energy diagram (IE, ΔE_{int}) which was obtained from four inhibitors of the test set. The decomposition of the IE into contributions from InhA active site residues is very useful for proposing relevant R groups that could enhance the binding affinity of PPZ analogs to MtInhA and, subsequently, improve the inhibitory potency. A comparative analysis of the EI calculated for the PPZs of the test set (Figure 3) broken down into three classes (highest activity

(PPZ1), moderate (PPZ5 and PPZ8) and lowest (PPZ12)) was carried out. to identify residues for which the contribution to binding affinity could be increased. However, comparative analysis showed approximately the same level of contribution to the EI of active site residues for all three classes of inhibitors. However, no suitable substitutions with the ability to improve binding affinity as previously reported for thymine-type inhibitors of the thymidine monophosphate kinase Mt design could be proposed²⁶. Based on this, we adopted a combinatorial approach for the design of novel PPZ analogues and screened *in silico* a virtual library of 310,500 PPZ analogues using the PH4 pharmacophore of InhA inhibition derived from the QSAR complexation model. As can be seen by EI analysis (Figure 3), the piperazine class (TS and VS)¹⁶ does not show obvious interaction energies with the residues of the hydrophobic pocket all around the aromatic ring.

3D-QSAR Pharmacophore Model

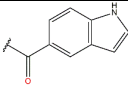
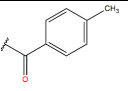
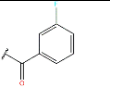
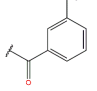
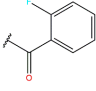
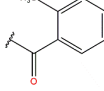
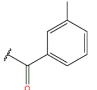
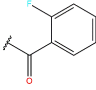
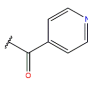
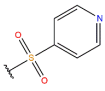
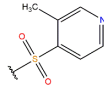
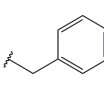
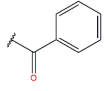
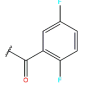
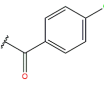
The molecular modeling program Discovery Studio²⁰ through its interaction generation protocol provides the characteristics of the pharmacophore of the active site of a protein. InhA mainly presents hydrophobic characteristics at the active site^{27,28,30}.

Table1: Training set (PPZ1-12) and validation set (PPV13-15) of InhA inhibitors used in the preparation of Quantitative Structure Activity Relation (QSAR) models of inhibitor binding.



Training set	ppz1	ppz2	ppz3
R			
IC_{50}^{Exp} (nM)	160	220	240
Training set	ppz4	ppz5	ppz6
R			
IC_{50}^{Exp} (μ M)	250	360	400
Training set	ppz7	ppz8	ppz9
R			
IC_{50}^{Exp} (μ M)	900	5990	9770
Training set	ppz10	ppz11	ppz12
R			
IC_{50}^{Exp} (μ M)	19960	50100	51000
Validation set	ppz1	ppz2	ppz3
R			
IC_{50}^{Exp} (μ M)	183	1570	1690

Table 2: Gibbs free energy (binding affinity) and its components for the training set of InhA inhibitors. PPZ1-12 and validation set inhibitors PPV13-15.

Training set	ppz1	ppz2	ppz3
R			
IC_{50}^{Exp} (nM)	160	220	240
Training set	ppz4	ppz5	ppz6
R			
IC_{50}^{Exp} (μM)	250	360	400
Training set	ppz7	ppz8	ppz9
R			
IC_{50}^{Exp} (μM)	900	5990	9770
Training set	ppz10	ppz11	ppz12
R			
IC_{50}^{Exp} (μM)	19960	50100	51000
Validation set	ppz1	ppz2	ppz3
R			
IC_{50}^{Exp} (μM)	183	1570	1690

^a for the chemical structures of the training set of inhibitors shown in Table 1; ^b M_w is the molecular mass of inhibitors; ^c $\Delta\Delta H_{MM}$ is the relative enthalpic contribution to the Gibbs free energy change related to enzyme-inhibitor (E:I) complex formation derived by molecular mechanics (MM): $\Delta\Delta H_{MM} = [E_{MM}\{E:I_x\} - E_{MM}\{I_x\}] - [E_{MM}\{E:I_{ref}\} - E_{MM}\{I_{ref}\}]$, I_{ref} is the reference inhibitor PPZ1; ^d $\Delta\Delta G_{sol}$ is the relative solvation Gibbs free energy contribution to the Gibbs free energy change of E:I complex formation: $\Delta\Delta G_{sol} = [G_{sol}\{E:I_x\} - G_{sol}\{I_x\}] - [G_{sol}\{E:I_{ref}\} - G_{sol}\{I_{ref}\}]$; ^e $\Delta\Delta TS_{vib}$ is the relative entropic contribution of inhibitor I_x to the Gibbs free energy related to E:I complex formation: $\Delta\Delta TS_{vib} = [\Delta\Delta TS_{vib}\{I_x\} - \Delta\Delta TS_{vib}\{I_{ref}\}]$; ^f $\Delta\Delta G_{com} = \Delta\Delta H_{MM} + \Delta\Delta G_{sol} - \Delta\Delta TS_{vib}$ is the relative Gibbs free energy change related to E:I complex formation; ^g IC_{50}^{Exp} is the experimental half-maximal inhibitory concentration of InhA inhibition obtained from reference; ^h Ratio of predicted and experimental half-maximal inhibition concentrations $pIC_{50}^{pre}/pIC_{50}^{exp}$ ($pIC_{50}^{pre} = \log_{10} IC_{50}^{pre}$) was predicted from computed $\Delta\Delta G_{com}$ using the regression equation for InhA shown in Table 3.

The high flexibility of the pocket due to the high mobility of the side chains Tyr158, Phe149 and the substrate binding loop (Thr196-Gly208) is often in the design of competitive substrate inhibitors⁴⁰.

Generation and validation of 3D-QSAR pharmacophore

The generation of the 3D-QSAR inhibitory pharmacophore of InhA was done based on the active conformations of the 12 PPZ1-12 training set and evaluated by the 3 PPV13-15 validation set covering a wide range of experimental activity (160 - 51000 nM). The generation process was performed in three main steps: constructive, subtractive and optimization¹⁹ as described earlier³⁰. PPZ1 in the constructive phase was retained as the main one because only its activity met the threshold criterion ($IC_{50}^{Exp} \leq 5/4 \times 160$ nM) and was used to generate the starting pharmacophore feature. Then in the subtractive phase. In the subtractive phase of the threshold criterion, compounds for which: $IC_{50}^{Exp} > 160 \times 10^{3.5}$ nM = 505 968 nM were considered inactive. According to this criterion, none of the PPZx in the training set was inactive and no starting PH4 feature was removed.

Finally the score of the pharmacophore hypotheses was improved during the optimization phase. These hypotheses were scored by taking into account the

errors in the activity estimates from regression and complexity via a simulated annealing approach. At the end of optimization, the top 10 pharmacophore hypotheses were retained, all of which had five-point characteristics. The cost values, correlation coefficients, root mean square deviation (RMSD) values, pharmacophore characteristics, and max-fit value of the top 10 hypotheses (Hypo1–Hypo10) are listed in Table 4. These hypotheses were selected based on significant statistical parameters, such as high correlation coefficient, low total cost, and low RMSD value. The generated pharmacophore models were then evaluated for their reliability based on the calculated cost parameters ranging from 51.9 (Hypo1) to 72.8 (Hypo10). The homogeneity of the generated hypotheses and the consistency of the PPZx TS is supported by the small and relative gap between the highest and lowest cost parameter. Then The fixed cost (32.01) is lower than the zero cost (579.53) by a difference $\Delta = 547.52$ for this pharmacophore model. This difference is a major quality indicator of the predictability of the PH4 ($\Delta > 70$ corresponds to an excellent chance or a probability greater than 90% that the model represents a strong correlation)¹⁹.

Table 3: Analysis of computed binding affinities $\Delta\Delta G_{com}$, its enthalpic component $\Delta\Delta H_{MM}$, and experimental half-maximal inhibitory concentrations $pIC_{50}^{exp} = -\log_{10}IC_{50}^{exp}$ of PPZs towards *MtInhA*.

Statistical Data of Linear Regression	(A)	(B)
$pIC_{50}^{exp} = -0.1506 \times \Delta\Delta H_{MM} + 6.8018$ (A)		
$pIC_{50}^{exp} = -0.1707 \times \Delta\Delta G_{com} + 8.7513$ (B)		
Number of compound n	12	12
Squared correlation coefficient of regression R^2	0.88	0.92
LOO cross-validated squared correlation coefficient R^2_{xv}	0.87	0.91
Standard error of regression σ	0.32	0.26
Statistical significance of regression. Fisher F-test	96.18	150.76
Level of statistical significance (%)	>95%	>95%
Range of activities IC_{50}^{exp} [nM]	160 – 51000	

The statistical data confirmed validity of the correlation equations (A) and (B) plotted on Figure 1. The ratio $pIC_{50}^{pre}/pIC_{50}^{exp} \cong 1$ (the pIC_{50}^{pre} values were estimated using correlation eq. B, Table 3) calculated for the validation set PPV13-15 documents the substantial predictive power of the complexation QSAR model from Table 2. Thus, the regression equation B (Table 3) and computed $\Delta\Delta G_{com}$ GFEs can be used for prediction of inhibitory potencies IC_{50}^{pre} against *MtInhA* for novel PPZ analogs, provided that they share the same binding mode as the training set piperazine PPZ1-12.

This difference is a major quality indicator of the PH4 predictability ($\Delta > 70$ corresponds to an excellent chance or a probability higher than 90% that the model represents a true correlation¹⁹). Statistically, a hypothesis to be significant must be close enough to the fixed cost and far enough from the zero cost. For the 10 hypotheses, the difference $\Delta \geq 506.68$, attests to the high quality of the pharmacophore model. Between

the different hypotheses, the standard indicators such as the RMSD covered from 1.75 to 2.60 and the squared correlation coefficient (R^2) is in an interval of 0.98 to 0.96. For a more in-depth analysis, the first hypothesis PH4 with the closest cost (51.9) to the fixed cost (32.01), the best RMSD and the best R^2 was retained.

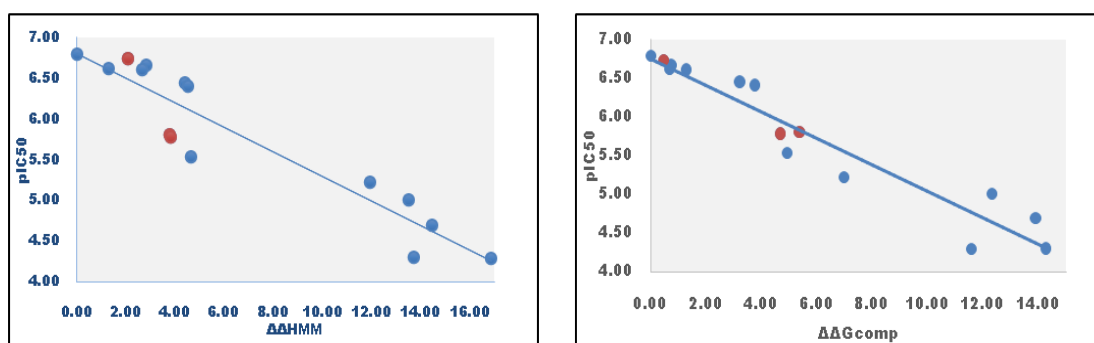


Figure 1: (A): plot of correlation equation between pIC_{50}^{exp} and relative enthalpic contribution to the GFE, $\Delta\Delta H_{MM}$ [kcal.mol⁻¹]. (B): Similar plot for relative complexation Gibbs free energies of the *InhA*-PPZx complex formation $\Delta\Delta G_{com}$ [kcal.mol⁻¹] of the training set.

The validation set data points are shown in orange color.

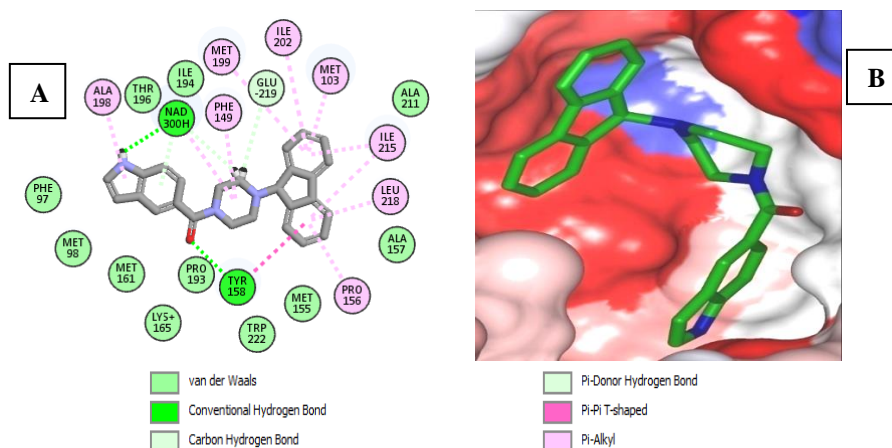


Figure 2: (A):2D schematic interaction diagram of the most potent inhibitor 1^{16} at the active site of *InhA* of *Mt*. (B): Connolly surface of the active site of *MtInhA* with bound most active designed PPZ 1 ($IC_{50}^{pre}=160M$).

The binding site surface is colored according to residue hydrophobicity: red - hydrophobic, blue - hydrophilic and white - intermediate.

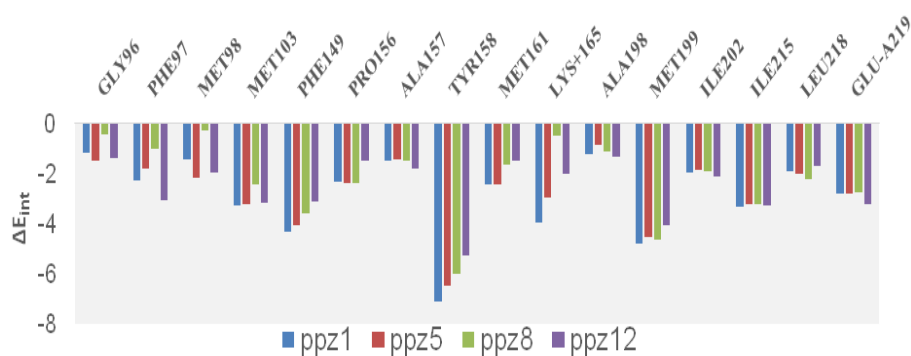


Figure 3: Molecular mechanics intermolecular interaction energy E_{int} breakdown to residue contributions in [kcal.mol⁻¹] for PPZ1 (160 nM), PPZ5 (360 nM), PPZ8 (5990 nM), PPZ12 (51000 nM).

Table 4: Parameters of 10 generated pharmacophoric hypotheses for InhA inhibitor after Cat- Scramble validation procedure (49 scrambled runs for each hypothesis at the selected level of confidence of 98%).

Hypothesis	RMSD ^a	R ^{2b}	Total costs ^c	Costs difference ^d	Closest Random ^e	Feature ^f
Hypo 1	1.75	0.98	51.9	527.58	66.1	HBA, HYD-Ar, HYD-Ar, HYD, HYD
Hypo 2	1.75	0.98	52.0	527.56	82.6	HBA, HYD-Ar, HYD, HYD, HYD
Hypo 3	1.80	0.98	54.0	525.54	105.7	HBA, HYD, HYD, HYD, HYD
Hypo 4	1.82	0.98	54.4	525.16	115.8	HBA, HYD-Ar, HYD, HYD, HYD
Hypo 5	2.00	0.98	57.4	522.09	120.5	HBA, HYD-Ar, HYD, HYD
Hypo 6	2.02	0.98	57.5	521.98	128.5	HBA, HYD-Ar, HYD-Ar, HYD
Hypo 7	1.99	0.98	57.6	521.92	133.3	HBA, HYD-Ar, HYD, HYD
Hypo 8	2.23	0.97	65.2	514.31	136.9	HBA, HYD, HYD, HYD
Hypo 9	2.39	0.97	68.2	511.32	140.3	HBA, HYD-Ar, HYD, HYD
Hypo 10	2.60	0.96	72.8	506.68	142.4	HBA, HYD, HYD, HYD
Fixed Cost	0	0	32.01			
Null Cost	9.64	0	579.53			

^aRoot Mean Square Deviation; ^bSquared correlation coefficient; ^c Overall cost parameter of the PH4; ^dCost difference between Null cost and hypothesis total cost; ^e Lowest cost from 49 scrambled runs at a selected level of confidence of 98%. ^fHBA (hydrogen-bond Acceptor); HYD (Hydrophobic). The Fixed Cost=32.01 with RMSD=0, Null Cost=579.53 with RMSD=9.64 and the Configuration cost=9.65

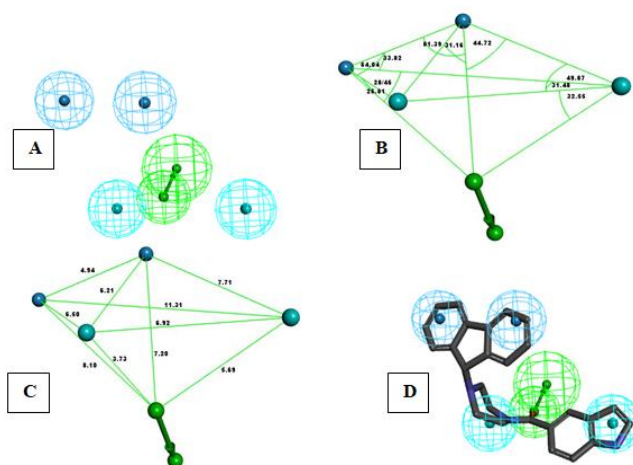


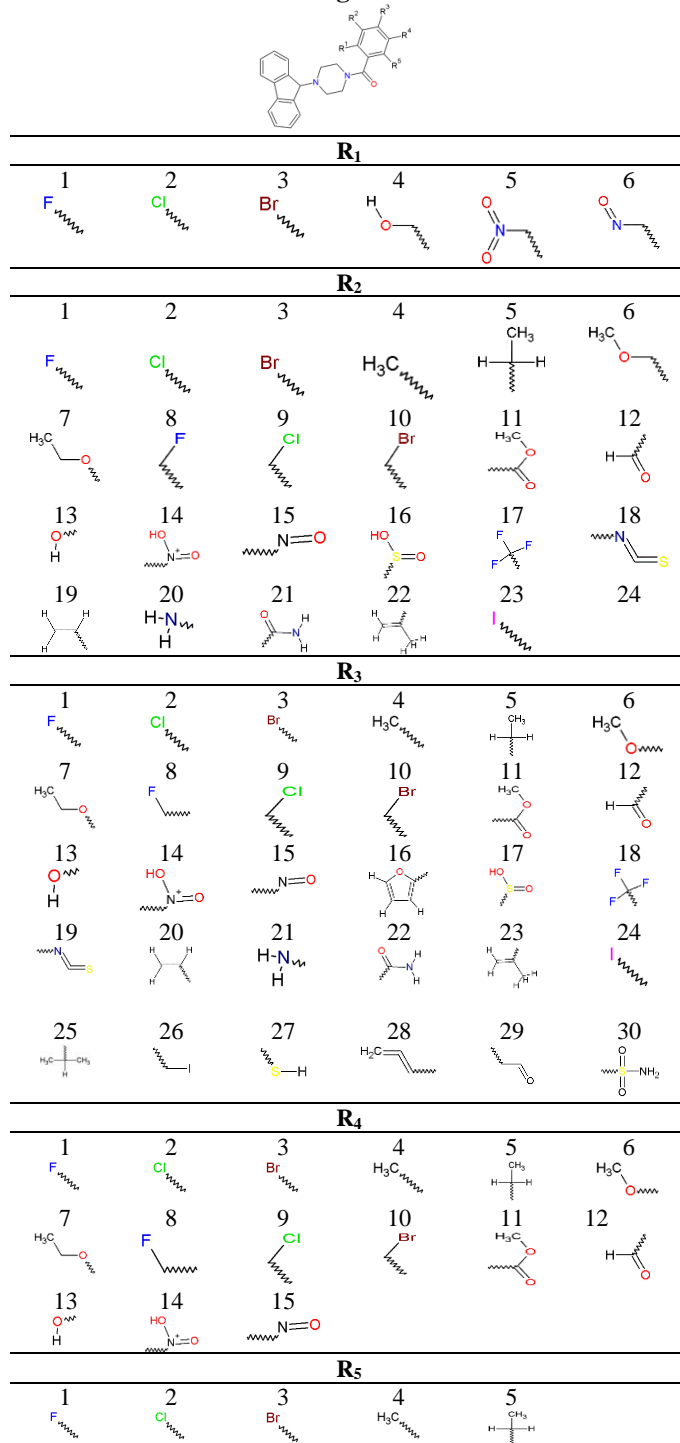
Figure 4: Pharmacophoric features. (A): coordinates of centers, (B and C): angles and distances of the centers, (D): mapping of the pharmacophore of InhA inhibitor with the most potent molecule PPZ1, (E): the correlation plot of experimental vs predicted inhibitory activity.

Feature legend: HYDA=Hydrophobic Aliphatic (blue), HYD=Hydrophobic (cyan), HBA=Hydrogen bond Acceptor (green)

The different statistical data for all the hypotheses (costs, RMSD, R²) are listed in Table 4. The configuration cost (9.65 for all hypotheses) far below 17 confirms this pharmacophore as a reasonable one. The regression equation for pK_i^{exp} vs. pK_i^{pre} estimated from Hypo1: pIC₅₀^{exp} = 0.9961 × pIC₅₀^{pre} + 0.0226 (n=12, R²=0.97, R²_{cv}=0.96, F-test=294, σ=0.18, α > 98%) is also plotted on Figure 4. Therefore, the

PH4 is good potentially to choose the new PPZ analogs. These parameters are in accordance with the OECD QSAR guidelines⁴¹. The predictive power of the pharmacophore model is assessed by calculating the ratio between the activities predicted by the PH4 model and those observed experimentally (pIC₅₀^{pre}/pIC₅₀^{exp}) for the whole set of compounds in the validation set (PPV13-15).

Table 5: R groups (fragments, substituent's) proposed for the design of the virtual library of PPZs analogues.



The high predictive power of the PH4 model regression is optimal and is demonstrated by the ratios that are all close to one. Another assessment of hypothesis 1 is the mapping of the PH4 binding mode in the 3D QSAR (Figure 4) of the most active PPZ1. We can perform computational design and selection of new PPZ analogues with high inhibitory potencies against MtnhA based on a strategy using the notable presence of hydrophobic features included in the best pharmacophore model.

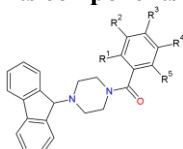
Virtual Screening

As demonstrated in our previous work²⁸ on inhibitor design, virtual screening of a virtual combinatorial

library can lead to the identification of positive hits of novel analogues.

Virtual library

Substitution of small fragments (R1 to R5) on the aromatic ring of the PPZ scaffold allowed the generation of an initial virtual combinatorial library based on the collected structural information¹⁶. All R groups present in Table 5 were attached to positions R1 to R5 of the PPZ scaffold to form a combinatorial library of the size: $R_1 \times R_2 \times R_3 \times R_4 \times R_5 = 6 \times 23 \times 30 \times 15 \times 5 = 310,500$ analogues. This initial diversity library was generated from building blocks (chemicals) listed in the databases of available chemicals⁴².

Table 6: GFE ($\Delta\Delta G_{\text{com}}$) complexation and its components for 50 top-scoring PPZ virtual analogues.

Designed analogs R ₁ - R ₅	M _w ^a [g·mol ⁻¹]	$\Delta\Delta H_{\text{MM}}$ ^b [kcal·mol ⁻¹]	$\Delta\Delta G_{\text{sol}}$ ^c [kcal·mol ⁻¹]	$\Delta\Delta T S_{\text{vib}}$ ^d [kcal·mol ⁻¹]	$\Delta\Delta G_{\text{com}}$ ^e [kcal·mol ⁻¹]	IC ₅₀ ^{pre f} [nM]	
N ^o	ppzl	393	0.00	0.00	0.00	0.00	160 ^E
1	1-4-21-1-4	419	2.23	-1.81	1.61	-1.18	111.34
2	1-8-1-11-1	498	1.57	-1.38	-4.41	4.60	1080.60
3	1-9-29-8-4	494	4.41	-1.60	-1.77	4.59	1077.43
4	1-5-21-1-1	451	0.44	-0.04	-3.22	3.62	734.97
5	1-12-5-12-4	456	-5.75	1.36	-1.53	-2.86	57.61
6	1-19-15-12-4	455	7.86	-3.09	-0.53	5.30	1421.31
7	1-20-4-8-4	433	3.18	-2.44	-0.35	1.08	271.27
8	1-19-21-13-2	463	-1.93	-2.07	0.22	-4.22	33.78
9	1-13-6-6-2	482	-1.94	0.90	-3.00	1.96	383.05
10	1-21-7-2-4	493	-13.73	1.78	-0.66	-11.29	2.10
11	2-11-21-2-4	496	2.05	-3.29	-4.43	3.18	619.76
12	2-1-21-7-1	483	-1.33	-1.13	-4.26	1.80	359.45
13	2-12-12-6-4	474	-3.16	-0.75	-5.23	1.32	298.21
14	2-12-15-6-1	493	-7.59	-1.80	-4.99	-4.40	31.47
15	2-12-7-12-4	488	-10.46	1.00	-0.12	-9.34	4.51
16	2-20-29-7-4	489	-14.26	0.07	1.56	-15.75	0.36
17	2-20-12-8-1	481	-3.86	-0.83	-2.76	-1.92	83.26
18	4-1-7-9-4	480	-13.59	0.54	0.10	-13.14	1.01
19	4-2-21-12-2	482	-4.66	0.00	-1.38	-3.28	48.76
20	4-1-29-4-4	444	-3.25	-1.38	0.20	-4.84	26.47
21	4-2-11-1-4	480	-0.51	-2.48	-0.01	-2.98	54.91
22	4-8-8-1-4	452	-10.02	-1.56	1.83	-13.41	0.91
23	4-9-6-8-4	480	-13.01	-0.56	0.52	-14.10	0.70
24	4-8-27-12-1	480	-9.43	-0.31	-0.37	-9.37	4.46
25	4-6-22-13-2	493	-8.01	2.86	-4.15	-1.00	119.68
26	4-6-29-7-4	486	-8.61	0.90	5.15	-12.86	1.13
27	4-7-21-2-4	463	4.69	-0.63	-0.77	4.83	1184.21
28	4-13-6-5-1	462	2.04	3.35	2.05	3.33	657.46
29	4-15-22-2-4	476	-3.98	3.28	-3.52	2.81	535.77
30	4-13-4-8-4	432	0.49	-0.46	0.12	-0.09	171.45
31	4-12-9-4-1	478	-6.29	2.27	-1.45	-2.56	64.80
32	4-15-7-6-1	491	-10.36	2.85	0.72	-8.23	6.98
33	4-20-9-13-4	449	-5.84	0.57	2.68	-7.94	7.81
34	4-20-2-7-2	498	-4.96	0.46	-4.23	-0.26	159.96
35	4-19-12-13-2	474	0.20	0.94	-2.77	3.92	827.69
36	4-20-7-6-2	493	-5.26	2.95	2.49	-4.81	26.81
37	4-20-5-12-1	459	-2.05	2.40	1.38	-1.04	117.77
38	4-20-8-1-1	453	-2.94	-0.23	-1.79	-1.37	103.31
39	4-22-21-8-4	457	8.60	-0.38	3.31	4.91	1222.27
40	4-22-29-6-4	482	-0.66	0.34	6.09	-6.41	14.29
41	4-22-29-15-4	481	-7.01	4.95	1.87	-3.93	37.81
42	4-22-22-2-4	487	2.78	1.20	2.49	1.50	319.13
43	4-22-21-13-2	475	8.43	1.26	0.53	9.17	6510.26
44	4-22-8-13-4	458	3.71	0.20	2.61	1.29	294.78
45	6-7-6-8-4	489	-1.84	0.59	0.00	-1.25	108.27
46	6-1-8-12-4	461	-3.34	1.84	-3.49	2.00	388.45
47	6-20-2-12-4	460	-3.00	2.06	-0.55	-0.39	152.02
48	6-21-7-5-4	498	-4.98	2.41	2.31	-4.88	26.00
49	6-20-13-5-1	460	1.70	0.78	-2.98	5.46	1514.82
50	6-20-27-4-4	444	-0.59	1.73	4.03	-2.89	56.86

Analog numbering concatenates the index of each substituent R₁ to R₅ with substituent numbers taken from Table 5.

^a M_w is the molar mass of the inhibitor; ^b $\Delta\Delta H_{\text{MM}}$ is the relative enthalpic contribution to the GFE change ($\Delta\Delta G_{\text{com}}$) of InhA -PPZ complex formation (for details, see Table 2); ^c $\Delta\Delta G_{\text{sol}}$ is the relative solvation GFE contribution to $\Delta\Delta G_{\text{com}}$; ^d $\Delta\Delta S_{\text{vib}}$ is the relative entropic (vibrational) contribution to $\Delta\Delta G_{\text{com}}$; ^e $\Delta\Delta G_{\text{com}}$ is the relative change in Gibbs free energy related to the formation of the InhA -PPZ protein-inhibitor complex $\Delta\Delta G_{\text{com}} \equiv \Delta\Delta H_{\text{MM}} - T\Delta\Delta S_{\text{vib}} + \Delta\Delta G_{\text{sol}}$.

Table 7: ADME-related properties of the best designed PPZ analogs and known antituberculous agents either in clinical use or currently undergoing clinical testing computed by QikProp.

FLAVs ^a	#Stars ^b	Mw ^c [g.mol ⁻¹]	Smol ^d [Å ²]	Smol, hfo ^e [Å ²]	Vmol ^f [Å ³]	RotB ^g	HBdon ^h	HBacc ⁱ	logPo/w ^j	logSwat ^k	logKHSA ^l	logB/B ^m	BIPcaco ⁿ [nm.s ⁻¹]	#mnda ^o	IC50pre ^p [nM]	HOA ^q HOAq	%HOA ^r
1-21-7-2-4	0	493	732.3	247.2	1410.0	4	2	8.25	3.7	-6.0	140.5	-0.4	0.7	3	2.10	3	87
2-12-7-12-4	0	488	770.8	284.9	1453.4	5	0	9.75	3.1	-5.1	126.4	-0.6	0.0	2	4.51	3	82
2-20-29-7-4	0	490	713.9	263.9	1409.4	6	1.5	8.75	3.6	-5.8	161.4	-0.4	0.5	5	0.36	3	87
4-1-7-9-4	0	480	715.7	286.0	1388.6	4	0	5.5	5.3	-6.9	530.6	0.2	1.0	4	1.01	3	93
4-8-8-1-4	0	452	676.9	220.5	1282.0	2	0	4.75	5.1	-6.6	570.6	0.4	1.0	4	0.91	3	93
4-9-6-8-4	0	480	709.6	263.4	1373.3	3	0	5.5	5.3	-6.9	606.9	0.4	1.0	5	0.70	3	95
4-8-27-12-1	0	480	684.3	194.2	1315.0	4	0	6.25	4.3	-6.5	227.2	-0.1	0.6	4	4.46	3	94
4-6-29-7-4	0	486	743.0	341.6	1457.8	7	0	8.25	3.6	-5.7	128.9	-0.7	0.3	5	1.13	3	86
4-15-7-6-1	0	491	717.9	295.9	1404.0	6	0	7.75	3.7	-6.0	170.6	-0.5	0.4	4	6.98	3	89
4-20-9-13-4	0	449	689.7	164.9	1307.4	4	2.5	6.5	3.6	-5.8	85.7	-0.6	0.7	6	7.81	3	82
Rifampin	1	137.1	314	0.0	480 *	2	-3	4.5	-0.7	0	-0.8	-0.8	267.5	2	-	2	67
Isoniazid	4	123.1	300	0.0	443 *	1	2	5	-0.6	-0.5	-0.8	-0.7	298.4	4	-	2	67
Ethambutol	2	204.3 *	476	395.8	806	11	4	6.4	-0.2	0.6	-0.8	0.0	107.8	4	-	2	62
Pyrazinamide	10	823.0 *	1090 *	850.0 *	2300 *	25 *	6	20.3 *	3.0	-3.1	-0.3	-2.7	38.2	11 *	-	1	34
Gatifloxacin	0	375.4 *	598	355.7	1093	2	1	6.8	0.5	-4.0	0	-0.6	17.0	1	-	2	52
Moxifloxacin	0	401.4	642	395.6	1168	2	1	6.8	1.0	-4.7	0.2	-0.6	20.9	1	-	2	56
Rifapentine	10	877.0	1025 *	844.9 *	2333 *	24 *	6	20.9 *	3.6	-2.2	-0.2	-1.5	224.0	13 *	-	1	51
Bedaquiline	4	555.5 *	787	213.7	1532	9	1	3.8	7.6 *	-6.9	1.7	0.4	1562.2	5	-	1	100
Delamanid	2	534.5	796	284.4	1470	7	0	6.0	5.8	-7.6	1.0	-1.0	590.9	2	-	1	85
Linezolid	0	337.4	555	337.2	996	2	1	8.7	0.6	-2.0	-0.7	-0.5	507.0	2	-	3	79
Sutezolid	1	353.4	594	330.6	1047	2	1	7.5	1.3	-3.4	-0.4	-0.4	449.3	0	-	3	82
Ofloxacin	1	361.4	581	337.0	1044	1	0	7.3	-0.4	-2.8	-0.5	-0.4	25.9	1	-	2	50
Amikacin	14	585.6	739	350.3	1500	22 *	17 *	26.9 *	-7.9 *	-0.2	-2.1	-3.5	0	14 *	-	1	0
Kanamycin	10	484.5	656	258.9	1291	17 *	15 *	22.7 *	-6.7 *	2.0	-1.4	-3.1	0	12 *	-	1	0
Imipenem	0	299.3	487	259.1	880	8	3	7.2	1.0	-1.8	-0.7	-1.4	35.0	3	-	3	61
Amoxicillin	2	365.4	561	164.6	1033	6	4.25	8.0	-2.5	-0.8	-1.1	-1.5	1.0	5	-	1	12
Clavulanate	0	199.2	397	184.6	630	4	2	6.5	-0.8	0.3	-1.3	-1.3	13.3	2	-	2	42

^a designed PPZ analogs and known antituberculosis agents, Table 6; ^b drug likeness, number of property descriptors (24 out of the full list of 49 descriptors of QikProp, ver. 3.7, release 14) that fall outside of the range of values for 95% of known drugs; ^c molar mass in [g.mol⁻¹] (range for 95% of drugs: 130–725 g.mol⁻¹) [46]; ^d total solvent-accessible molecular surface, in [Å²] (probe radius 1.4 Å) (range for 95% of drugs: 300–1000 Å²); ^e hydrophobic portion of the solvent-accessible molecular surface, in [Å²] (probe radius 1.4 Å) (range for 95% of drugs: 0–750 Å²); ^f total volume of molecule enclosed by solvent-accessible molecular surface, in [Å³] (probe radius 1.4 Å) (range for 95% of drugs: 500–2000 Å³); ^g number of non-trivial (not CX3), non-hindered (not alkene, amide, small ring) rotatable bonds (range for 95% of drugs: 0–15); ^h estimated number of hydrogen bonds that would be donated by the solute to water molecules in an aqueous solution. Values are averages taken over several configurations, so they can assume non-integer values (range for 95% of drugs: 0.0–6.0); ⁱ estimated the number of hydrogen bonds that would be accepted by the solute from water molecules in an aqueous solution. Values are averages taken over a number of configurations, so they can assume non-integer values (range for 95% of drugs: 2.0–20.0); ^j logarithm of partitioning coefficient between n-octanol and water (o/w) phases (range for 95% of drugs: -2–6.5); ^k logarithm of predicted aqueous (wat) solubility, logS. S in mol dm⁻³ is the concentration of the solute in a saturated solution that is in equilibrium with the crystalline solid (range for 95% of drugs: -6.0–0.5); ^l logarithm of predicted binding constant to human serum albumin (range for 95% of drugs: -1.5 to 1.5); ^m logarithm of predicted brain/blood partition coefficient (range for 95% of drugs: -3.0 to 1.2); ⁿ predicted apparent Caco-2 cell membrane permeability in Boehringer-Ingelheim scale in [nm s⁻¹] (range for 95% of drugs: < 25 poor, > 500 nm s⁻¹ great); ^o number of likely metabolic reactions (range for 95% of drugs: 1–8); ^p predicted constants IC₅₀^{pre}, was predicted from computed ΔΔG_{com} using the regression Equation (B) shown in (Table 3); ^q human oral absorption (1=low, 2=medium, 3=high); ^r percentage of human oral absorption in gastrointestinal tract (<25%=poor, >80%=high); * star in any column indicates that the property descriptor value of the compound falls outside the range of values for 95% of known drugs.

The introduction of a set of filters and penalties such as Lipinski's rule of 5 allowed obtaining a reduced size of the library containing increased drug-like molecules⁴³ which led to selecting a smaller number of suitable

PPZs that could be subjected to *in silico* screening. This focus allowed reducing the size of the initial library to 19,044 analogues, or 6% of its initial size.

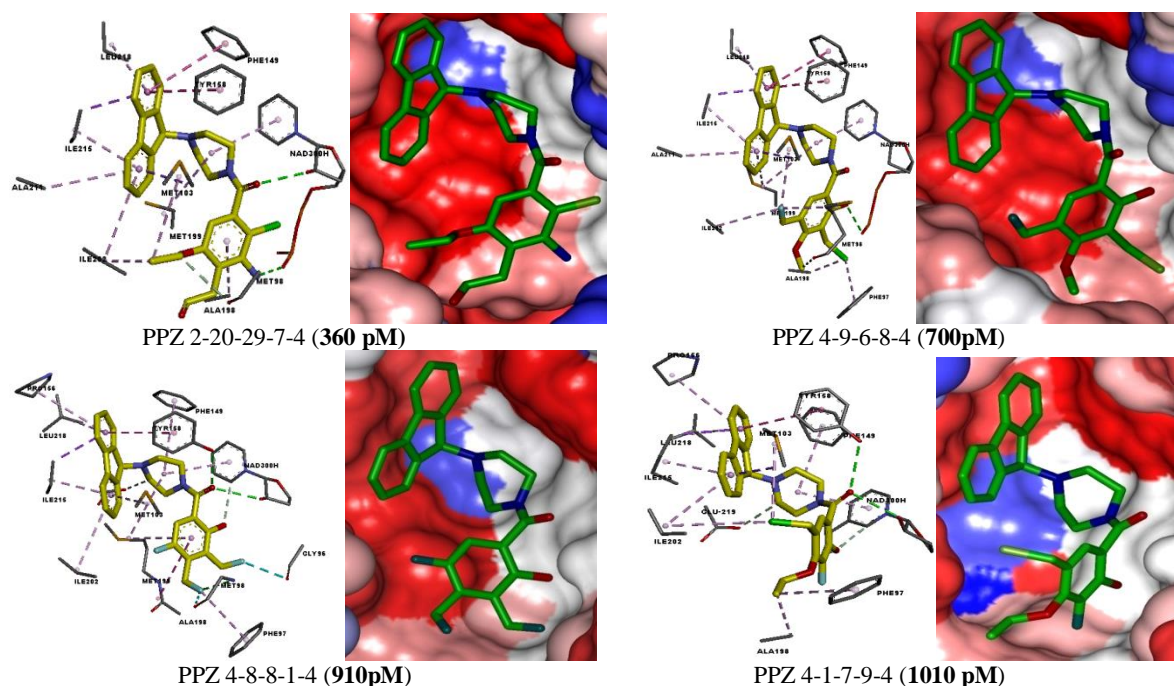


Figure 5: (left), Close-up of the virtual response of the four new potential developed analogues PPZ 2-20-29-7-4, PPZ 4-9-6-8-4, PPZ 4-8-8-1-4 and PPZ 4-1-7-9-4 in active site InhA and (right), their respective conolly surface.

The binding site surface is colored according to residue hydrophobicity: red—hydrophobic, blue—hydrophilic, and white.

Virtual screening of library of PPZs

For a more detailed examination for molecular structures matching the 3D-QSAR PH4 Hypo1 pharmacophore model of InhA inhibition the screening of 19044 analogues was performed. 60 PPZs were mapped to at least 4 pharmacophore features, 50 of which mapped to at least 5 pharmacophore features. These best-fit analogues (PH4 hits) were then subjected to complexation QSAR model screening. The calculated GFE of InhA-PPZx complex formation, their components and predicted half-maximal inhibitory concentrations IC_{50pre} calculated from correlation equation B (Table 3), are listed in Table 6.

Analysis of Novel PPZs inhibitors

Histograms of the frequency of occurrence of R_1 , R_2 , R_3 , R_4 and R_5 among the top 50 PH4 hits (Figure 5) were prepared in order to identify which substituents lead to new inhibitor candidates with the highest predicted potencies towards Mt InhA. The histograms

show that the R_1 groups 1 and 4 were represented respectively with the highest frequency of occurrence (10) and (27) among the 50 hits; the R_2 groups: 12 (5); 22 (6); 20 (11); R_3 groups : 7, 29, (6) and 21 (9); R_4 groups : 1 (5) and 2, 7 (4) and 12, 13 (6) and 8 (7); R_5 groups : 1(12) and 2(7) and 3 (30). The top ten scoring virtual hits namely analogs are: 1-21-7-2-4 ($IC_{50pre}=2100$ pM), 2-12-7-12-4 (4510 pM), 2-20-29-7-4 (360 pM), 4-1-7-9-4 (1010 pM), 4-8-8-1-4 (910 pM), 4-9-6-8-4 (700 pM), 4-8-27-12-1 (4460 pM), 4-6-29-7-4 (1130 pM), 4-15-7-6-1(6980 pM) and 4-20-9-13-4 (7810 pM). These analogues include mostly the following substituents at R_1 position: 1, 2, 4; R_2 position : 21, 12, 20, 18, 9, 6, 15; R_3 position : 7, 29, 8, 6, 27, 7, 9; R_4 groups : 2, 12, 7, 9, 1, 8, 6, 13; R_5 groups : 4, 1. The larger hydrophobic pocket due to its amino acid composition all R groups display preferences for shorter aliphatic building blocks as shown in Table 5.

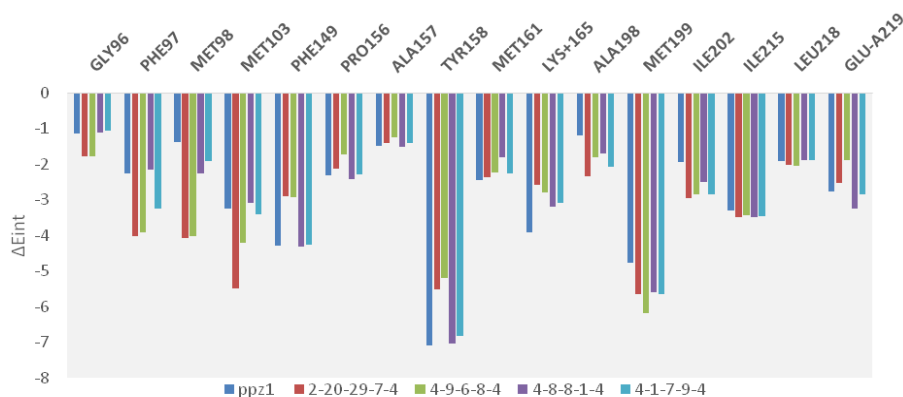


Figure 6: Molecular mechanics intermolecular interaction energy E_{int} breakdown to residue contributions, in $[kcal.mol^{-1}]$ shown for the four best designed novel PPZ analogs and PPZ1, most active ligand of training set.

The color coding refers to ligands and is given in the legend

There is an overall increase in the binding affinity of InhA for substitutions in the R1 to R5 positions of PPZs as illustrated by the inhibitory potencies of the majority of the newly designed analogues. The best designed PPZ benzamide 2-20-29-7-4 displays a predicted minimum inhibitory concentration of $IC_{50}^{pre}=360$ pM which is more than 100-fold lower than that of the most active compound in the TS, PPZ1 with $IC_{50}^{exp}=160$ nM (Figure 6).

ADME Profiles of Designed PPZs

Pharmacokinetic profile obtained of InhA inhibitors still requires increased research. Presented in Table 7, the ADME of our new analogs, were described earlier by the QikProp program⁴⁴ taken from the method of Jorgensen⁴⁵. The fundamental principles of this method are described previously²⁴. Our best analogs are compared with that of drugs used on the market to treat tuberculosis disease (Table 7).

DISCUSSION

A training set of 12 PPZs and validation set of 3 PPZs (Table1) were selected from a heterogeneous series of InhA inhibitors for which experimentally determined inhibitory activities were available from a single laboratory¹⁶. Both were obtained by synthesizing from the 1-(9H-fluoren-9-yl)-piperazine. The first one is from the synthesis bearing modifications around the carbonyl hydrogen bond acceptor using 1-(9H-fluoren-9-yl)-piperazine and the second group were from direct sulfonylation. The whole series was obtained by substitutions at five positions of the aromatic ring of the other side of the sulfonyl and carbonyl surrounded by hydrophobic residues constituted of residues Pro 99, Gly 104, Met 103, Tyr 158, Phe 149 and Met 161, Met 98, Ala 198 of Genz-10850 (PPZ1) as shown in Table1. Their experimental inhibitory concentrations IC_{50}^{exp16} cover a concentration range sufficiently wide to serve well for building of a reliable QSAR model of InhA inhibition. According to the structures of PPZ8 and PPZ5 studied, the presence of the methyl group at the C2 position of the aryl moiety causes steric hindrance due to the restricted space in the cavity formed by Met103, Tyr158, and Met161 residues of MtInhA¹⁶. In order to identify structural modifications of the aromatic ring leading to increased binding affinity of PPZs to InhA of *Mt*b we have carried out detailed analysis of interactions in a series of InhA-PPZs complexes with help of the complexation QSAR model. The first step of this analysis aimed at obtaining insight into InhA active-site interactions by performing the interaction energy breakdown into contributions from individual residues filling the hydrophobic pocket displayed on Figure 3 for the most active inhibitor PPZ1, moderate active (PPZ5 and PPZ8) and the lowest (PPZ12) activity, Table 2¹⁶. Figure 4 showed that there is no too difference concerning the interaction Energy (IE) between the three classes of activity. To obtain the best analogs PPZ we proceed by a combinatorial library. As the pocket containing the R₁ groups and formed by Met103, Tyr158, and Met161 is too small we put their short substituents. We notice that

the analogs dominated by small fragment like halogenure and hydroxyd have the most frequency of occurrence. The convenient size of the fragment chosen led to obtain the best analogs considerably most active than the most active of the training and the validation sets. The most four virtual active analogs were PPZ 2-20-29-7-4 ($IC_{50}^{pre}=360$ pM), PPZ 4-9-6-8-4 ($IC_{50}^{pre}=700$ pM), PPZ 4-8-8-1-4 ($IC_{50}^{pre}=910$ pM) and PPZ 4-1-7-9-4 ($IC_{50}^{pre}=1010$ pM) with favorable predicted pharmacokinetic profile than the older currently used drugs. We can suggest them for synthesis.

CONCLUSION AND RECOMMENDATION

In this work the crystallographic structure of the InhA-PPZ1 (1P44) complex and the structural properties of the Piperazine derivatives identified by Mariane Rotta *et al.*¹⁶, as a potential antituberculosis agent and whose target is InhA enabled us to develop a QSAR complexation model capable of explaining more than 92% of the variation in the experimental inhibitory activity of Piperazine derivatives by the Gibbs free energy of formation of the InhA-PPZx complex. Following this QSAR model, we obtained a 3D-QSAR PH4 pharmacophore model using a training set of 12 PPZs and a validation set of 3 PPZs with known inhibitory activities¹⁶. The visual analysis and calculation of the interactions between InhA and PPZs in the active site of the enzyme guided us in the design of a virtual combinatorial library of new PPZ analogs with a substitution on the scaffold at the position R₁ to R₅ on the aromatic ring. The virtual library obtained was first focused by considering Lipinski's five rule and then screened by the 3D QSAR pharmacophore identified during chemical space exploration around R₁ to R₅ positions novel PPZs analogs by the QSAR complexation model with predicted picomolar *Mt*InhA inhibitory potencies PPZ 2-20-29-7-4 ($IC_{50}^{pre}=360$ pM), PPZ 4-9-6-8-4 ($IC_{50}^{pre}=700$ pM), PPZ 4-8-8-1-4 ($IC_{50}^{pre}=910$ pM) and PPZ 4-1-7-9-4 ($IC_{50}^{pre}=1010$ pM) all display also favorable pharmacokinetic profiles compared to current antituberculars. We believe that they are worth synthesizing and evaluating.

ACKNOWLEDGEMENTS

The authors would like to thank the Laboratory of Fundamental and Applied Physics at NANGUI ABROGOUA University, in Côte d'Ivoire, for providing the facilities necessary for this work.

AUTHOR'S CONTRIBUTION

Kouman C: performed the complexation study, PH4 pharmacophore generation, interaction energy analysis, the PH4-based VL searching and the analogues evaluation. **Kouassi F:** established the first preliminary complexation model in order to confirm the feasibility of this work. **Fagnidi H:** performed the VL generation and focusing and wrote original draft, methodology, investigation. **Kéita M:** editing, review. **Fofana I:** performed the VL generation and focusing. **Allangba**

G: formal analysis. **Megnassan E:** writing, review, and editing, data curation. All authors read and approved the final manuscript for publication.

DATA AVAILABILITY

Data will be available on request to anyone from the correspondence author.

CONFLICT OF INTERESTS

The authors declared no conflict of interests

REFERENCES

- Global tuberculosis report 2024. Geneva: World Health Organization; 2024. Licence: CC BY-NC-SA 3.0 IGO
- Koul A, Arnoult E, Lounis N, Guillemont J, Andries K. The challenge of new drug discovery for tuberculosis. *Nature*. 2011; 469(7331):483–90. <https://doi.org/10.1038/nature09657>
- Palomino JC, Martin A. TMC207 becomes bedaquiline, a new anti-TB drug. *Future Microbiol*. 2013;8(9):1071–80. <https://doi.org/10.2217/fmb.13.85>
- Vilcheze, C.; Morbidoni, H.R.; Weisbrod, T.R.; et al. Inactivation of the InhA-encoded fatty acid synthase II (FASII) enoyl-acyl carrier protein reductase induces accumulation of the FASI end products and cell lysis of *Mycobacterium smegmatis*. *J. Bacteriol* 2000, 182, 4059–4067. <https://doi.org/10.1128/JB.182.14.4059-4067.2000>
- Aguero F, Al-Lazikani B, Aslett M, et al. Genomic-scale prioritization of drug targets: The TDR Targets database. *Nat Rev Drug Discov* 2008, 7, 900–907. <https://doi.org/10.1038/nrd2684>
- Campbell JW, Cronan JE. Bacterial fatty acid biosynthesis: Targets for antibacterial drug discovery. *Annu Rev Microbiol* 2001, 55, 305–332 <https://doi.org/10.1146/annurev.micro.55.1.305>
- Udwadia ZF, Amale RA, AjbaniKK, Rodrigues C. Totally drug-resistant tuberculosis in India. *Clin Infect Dis* 2012;54(4):579–81. <https://doi.org/10.1093/cid/cir889>
- Timmins, G.S.; Deretic, V. Mechanisms of action of isoniazid. *Mol. Microbiol*. 2006, 62, 1220–1227. <https://doi.org/10.1111/j.1365-2958.2006.05467.x>
- Freundlich JS, Wang F, Vilcheze C, et al. Triclosan derivatives: towards potent inhibitors of drug-sensitive and drug resistant *Mycobacterium tuberculosis*. *Chem Med Chem* 2009;4(2):241–48. <https://doi.org/10.1002/cmdc.200800261>
- Am Ende CW, Knudson SE, Liu N, et al. Synthesis and *in vitro* antimycobacterial activity of B-ring modified diaryl ether InhA inhibitors. *Bioorg Med Chem Lett* 2008, 18, 3029–3033. <https://doi.org/10.1016/j.bmc.2008.04.038>
- Luckner SR, Liu N, Am Ende CW, et al. A slow, tight binding inhibitor of InhA, the enoyl-acyl carrier protein reductase from *Mycobacterium tuberculosis*. *J Biol Chem* 2010; 285: 14330–14337. <https://doi.org/10.1074/jbc.M109.090373>
- He X, Alian A, Stroud R, de Montellano PR. Pyrrolidinecarboxamides as a novel class of inhibitors of enoyl acyl carrier protein reductase from *Mycobacterium tuberculosis*. *J Med Chem* 2006; 49: 6308–6323 <https://doi.org/10.1021/jm060715y>
- He X, Alian A, de Montellano P.R. Inhibition of the *Mycobacterium tuberculosis* enoyl acyl carrier protein reductase InhA by arylamides. *Bioorg Med Chem* 2007; 15: 6649–6658. <https://doi.org/10.1016/j.bmc.2007.08.013>
- Guardia A, Gulten G, Fernandez R, et al. N-Benzyl-4-(heteroaryl)methylbenzamides: A new class of direct NADH-dependent 2-trans enoyl-acyl carrier protein reductase (InhA) inhibitors with antitubercular activity. *Chem Med Chem* 2016; 11: 687–701. <https://doi.org/10.1002/cmdc.201600020>
- Shirude PS, Madhavapeddi P, Naik M, et al. Methylthiazoles: A novel mode of inhibition with the potential to develop novel inhibitors targeting InhA in *Mycobacterium tuberculosis*. *J Med Chem* 2013;56(21):8533–42. <https://doi.org/10.1021/jm4012033>
- Rotta M, Timmers M, Pissinate K, et al. Piperazine derivatives: Synthesis, inhibition of the *Mycobacterium tuberculosis* enoyl-acyl carrier protein reductase and SAR studies. *European J Med Chem* 2015; 90:436-447. <https://doi.org/10.1016/j.ejmech.2014.11.034>
- Punkvang A, Kamsri P, Kumkong A, et al. The structural requirement of direct InhA inhibitors for high potency against *M. tuberculosis* based on computer aided molecular design, Science against microbial pathogens: communicating current research and technological advances, A. Mendez-Vilas (Ed.), Microbiology Book Series No. 3, Formatex Research Center, Badajoz, Spain, 2011, pp. 160-168.
- Berman HM, Westbrook J, Feng Z, Gilliland G, Bhat TN, Weissig H, Shindyalov IN, Bourne PE. The protein data bank. *Nucl. Acids Res* 2000; 28:235-242. <https://doi.org/10.1107/s0907444902003451>
- Discovery Studio molecular modeling and simulation program version 2.5, Accelrys, Inc., San Diego, CA, 92121, USA, 2009
- OwonoOwono LC, Keita M, Megnassan E, Frecer V, Miertus S. Design of thymidine analogues targeting thymidilate kinase of *Mycobacterium tuberculosis*. *Tuberculosis Res Treat* 2013;670836. <https://doi.org/10.1155/2013/670836>
- Frecer V, Miertus S, Tossi A, Romeo D. Rational design of inhibitors for drug-resistant HIV-1 aspartic protease mutants. *Drug Des Discov* 1998;15(4):211-231
- Frecer V, Miertus S. Interactions of ligands with macromolecules: rational design of specific inhibitors of aspartic protease of HIV-1. *Macromol Chem Phys* 2002;203:1650–1657. <https://doi.org/10.1002/15213935>
- Frecer V, Berti F, Benedetti F, Miertus S. Design of peptidomimetic inhibitors of aspartic protease of HIV-1 containing -Phe Psi Pro- core and displaying favourable ADME-related properties. *J Mol Graph Model* 2008;27(3):376-387. <https://doi.org/10.1016/j.jmgm.2008.06.006>
- Dali B, Keita M, Megnassan E, Frecer V, Miertus S. Insight into selectivity of peptidomimetic inhibitors with modified statine core for plasmepsin II of *Plasmodium falciparum* over human cathepsin D. *Chem Biol Drug Des*. 2012;79(4):411-430. <https://doi.org/10.1111/j.17470285.2011.01276.x>
- Megnassan E, Keita M, Bieri C, Esmel A, Frecer V, Miertus S. Design of novel dihydroxynaphthoic acid inhibitors of *Plasmodium falciparum* Lactate Dehydrogenase. *Med Chem* 2012, 8, 970-984. <https://doi.org/10.2174/157340612802084324>
- Keita M, Kumar A, Dali B, et al. Quantitative structure-activity relationships and design of thymine-like inhibitors of thymidine monophosphate kinase of *Mycobacterium tuberculosis* with favourable pharmacokinetic profiles. *RSC Adv*. 2014, 4, 55853-55866. <https://doi.org/10.1039/c4ra06917j>
- Owono Owono LC, Ntie-Kang F, Keita M, et al. Virtually designed triclosan-based inhibitors of enoyl-acyl carrier protein reductase of *Mycobacterium tuberculosis* and of *Plasmodium falciparum*. *Mol Inform* 2015, 34, 292–307. <https://doi.org/10.1002/minf.201400141>
- Kouassi AF, Kone M, Keita M, et al. Computer-aided design of orally bioavailable pyrrolidinecarboxamide inhibitors of Enoyl-Acyl carrier protein reductase of *Mycobacterium tuberculosis* with favorable pharmacokinetic profiles. *Int J Mol Sci* 2015, 16, 29744-29771. <https://doi.org/10.3390/ijms161226196>

29. Allangba KNPG, Keita M, Frecer V, *et al.* Virtual design of novel *Plasmodium falciparum* cysteine protease falcipain-2 hybrid lactone-chalcone and isatin-chalcone inhibitors probing the S2 active site pocket. *J Enz Inhib Med Chem* 2018; 34: 547-561.
<https://doi.org/10.1080/14756366.2018.1564288>
30. Kouman KC, Keita M, N'Guessan KR, *et al.* Structure-based design and *in silico* screening of virtual combinatorial library of benzamides inhibiting 2-transEnoyl-acyl carrier protein reductase of *Mycobacterium tuberculosis* with favourable predicted pharmacokinetic profiles. *Int J Mol Sci* 2019; 20:4730.
<https://doi.org/10.3390/ijms20194730>
31. N'Guessan H, Soro I, Keita M, Megnassan E. Design and *in silico* screening of combinatorial library of new herbicidalanalogs of cycloalka[d]quinazoline-2,4dione-benzoxazinones inhibiting protoporphyrino-gen ix oxidase. *J Pharm Res Int* 2022;34(56):42-61.
<https://doi.org/10.9734/jpri/2022/v34i567251>
32. Djako B, Keita M, Bisseyou Y, Esmel A, Megnassan E. Computer-assisted design of novel polyketide synthase 13 of *Mycobacterium tuberculosis* inhibitors using molecular modeling and virtual screening. *J Pharm Res Int* 2022;34(56):12- 41.
<https://doi.org/10.9734/jpri/2022/v34i567250>
33. Bieri C, Esmel A, Keita M, *et al.* Structure-based design and pharmacophore-based virtual screening of combinatorial library of triclosan analogues active against enoyl-acyl carrier protein reductase of *Plasmodium falciparum* with favourable ADME profiles. *Int J Mol Sci* 2023;24(8): 6916.
<https://doi.org/10.3390/ijms24086916>
34. Kone M, N'Guessan H, N'Gouan AJ, MKoblavi F, Megnassan E. Computer-aided design of new hydroxamic acid derivatives targeting the *Plasmodium falciparum* M17 metallo-aminopeptidase with favorable pharmacokinetic profile. *Int J Pharm Sci Drug Res* 2023;15(3):356-375.
<https://doi.org/10.25004/IJPSDR.2023.150317>
35. Ziki E, Akonan L, Kouman KC, *et al.* Virtual design of novel coumarinyl substituted sulfonamide inhibitors of carbonic anhydrase II as potential drugs against glaucoma. *J Pharm Res Int* 2023; 35(24): 10-33.
<https://doi.org/10.9734/JPRI/2023/v35i247424>
36. Saura J, Kettler R, Da Prada M, Richards JG. Quantitative enzyme radioautography with 3H-Ro 41-I 049 and 3H-Ro 19-6327 *in vitro*: Localization and abundance of MAOA and MAO-B in rat CNS, peripheral organs, and human brain. *J. Neurosci* 1992; 12(5):1977-1999.
<https://doi.org/10.1523/JNEUROSCI.12-0501977.1992>
37. Lee J, Natalie B, Drinkwater N, *et al.* Novel Human Aminopeptidase N Inhibitors: Discovery and optimization of subsite binding interactions. *J Med. Chem* 2019; 62(15): 7185-7209.
<https://doi.org/10.1021/acs.jmedchem.9b00757>
38. He X, Alian A, Stroud R, Ortiz de Montellano PR. Pyrrolidine carboxamides as a novel class of inhibitors of enoyl acyl carrier protein reductase from *Mycobacterium tuberculosis*. *J Med Chem* 49 (21) (2006) 6308 – 6323.
<https://doi.org/10.1021/jm060715y>
39. Kuo MR, Morbidoni HR, Alland D, *et al.* Targeting tuberculosis and malaria through inhibition of enoylreductase: compound activity and structural data, *J Biol Chem* 2003; 278 (23):20851e20859.
<https://doi.org/10.1074/jbc.M211968200>
40. Sullivan TJ, Truglio JJ, Boyne ME, *et al.* High affinity InhA inhibitors with activity against drug-resistant strains of *Mycobacterium tuberculosis*. *ACS Chem Biol* 2006; 1: 43–53. <https://doi.org/10.1021/cb0500042>
41. OECD (2014), Guidance Document on the Validation of (Quantitative) Structure-Activity Relationship [(Q)SAR] Models, OECD Series on Testing and Assessment, No. 69, OECD Publishing, Paris.
<https://doi.org/10.1787/9789264085442-en>
42. Available Chemicals Directory, Version 95.1, MDL Information Systems, San Leandro, CA
43. Lipinski CA, Lombardo F, Dominy BW, Feeney PJ. Experimental and computational approaches to estimate solubility and permeability in drug discovery and development settings. *Adv Drug Deliv Rev* 2001; 46, 3–26. [https://doi.org/10.1016/S0169-409X\(00\)00129-0](https://doi.org/10.1016/S0169-409X(00)00129-0)
44. Qik Prop, version 3.7, release 14; XSchrödinger, LLC: New York, NY; 2014
45. Jorgensen WL, Duffy EM. Prediction of drug solubility from montecarlo simulations. *Bioorg Med Chem Let.* 2000;10:1155-1158
[https://doi.org/10.1016/S0960-894X\(00\)00172-4](https://doi.org/10.1016/S0960-894X(00)00172-4)